In-situ imaging of inter- and intra-laminar damage in open-hole tension tests of carbon fibre-reinforced composites

Fatih E. Oz[1], Mahoor Mehdikhani[2], Nuri Ersoy[3], Stepan V. Lomov[2]

[1]Istanbul Şehir University, Department of Mechanical Engineering, Dragos, 34865, Istanbul, Turkey
[2]KU Leuven, Department of Materials Engineering, Kasteelpark Arenberg 44, 3001 Leuven, Belgium
[3]Boğaziçi University, Department of Mechanical Engineering, Bebek, 34342, Istanbul, Turkey
E-mails: fatihertugruloz@sehir.edu.tr, mahoor.mehdikhani@kuleuven.be, nuri.ersoy@boun.edu.tr, stepan.lomov@kuleuven.be

ABSTRACT

This paper investigates damage progression during Open-Hole Tension (OHT) test of carbon fibre-reinforced composites with different Quasi-Isotropic (QI) layups. Digital Image Correlation (DIC) and *in-situ* edge microscopy are utilized simultaneously to detect damage on the specimen's surface and in the inner plies, respectively. It is found that damage does not always initiate in the 90° plies, but also in the surface 45° plies, depending on the orientation of the adjacent ply. DIC resulting strain field on the surface does not necessarily have the same butterfly-shape concentration around the hole, in all layups. Some laminates show large free edge delaminations at 45°/90° interfaces. This study adds *in-situ* evidences to the existing data on damage during OHT test of QI laminates, providing quantitative and comparative information on different damage modes, and reveals new features of the damage phenomena.

Keywords: carbon fibre; polymer-matrix composites (PMCs); open-hole tension (OHT); damage mechanics; non-destructive testing; digital image correlation (DIC); optical microscopy

1. INTRODUCTION

Mechanical damage in composite materials has complex modes including matrix cracking, fibre/matrix debonding, delamination, and fibre breakage. Damage is more complicated in Quasi-Isotropic (QI) laminates than that in UniDirectional (UD) and Cross-Ply (XP) laminates due to a high number of different ply orientations, which causes occurrence of various damage modes in the different plies. The presence of a hole in a specimen during an Open-Hole Tension (OHT) test, causes considerable changes in the mechanical behaviour and damage mechanisms, compared to a plain tension test.

Wisnom, Hallet and colleagues [1–4] carried out a large experimental and numerical programme to investigate the effect of geometry and ply scaling on strength and damage evolution during OHT tests of QI Carbon Fibre-Reinforced Plastic (CFRP) composites, with post-mortem damage observation. Large load drops in the load-displacement curves of $[+45_2/90_2/-45_2/0_2]_s$ and $[+45_4/90_4/-45_4/0_4]_s$ laminates were attributed to delaminations at the -45°/0° interfaces, revealed by the post-mortem free edge observation after the first major drop [1]. Initiation and evolution of intra- and inter-laminar damage modes in the same laminate types were investigated with post-mortem X-Ray radiography of the interrupted-test specimens as well as finite element models [3,4].

In order to broaden the understanding of damage progression during OHT tests, Nixon-Pearson et al. [5,6] used post-mortem micro-Computed Tomography (micro-CT) technique to obtain damage patterns through the thickness of $[+45_2/90_2/-45_2/0_2]_s$ laminates. Observations of the interrupted-test specimens at 60 %, 70 % and 80 % of the Ultimate Tensile Strength (UTS) provided a correlation with the previously reported damage progressions in [3,4]. However, these observations were still not full since only intra-laminar damage modes were detected. In order to fully characterize the damage modes and correlate them with stress-strain curves, more interruptions are required, but it takes too much time to analyse results.

For example, the application of dye penetrant for clear observation of damage can take two days [5,6].

Even though aforementioned *ex-situ* micro-CT can identify the damage in different plies with high resolution, it does not provide *in-situ* observations. As an *in-situ* optical observation technique, Moiré interferometry was used for damage detection in OHT tests of composite specimens [7,8]. However, identification of damage in the inner plies is not possible with this method.

On the other hand, Digital Image Correlation (DIC), i.e. a non-contact full-field measurement technique, applied to the *in-situ* images of the specimen during loading, can detect damage in composites by means of the strain localizations caused by the damage. Using DIC, it is possible to detect transverse cracks in 90° plies, longitudinal fibre/matrix splitting in 0° plies and off-axis cracks in ±45° plies during OHT tests of UD and angle-ply biaxial laminates [9–11]. DIC is also used to detect first ply failure on surface plies and investigate the damage progression in more complex laminates [9–17]. Micro-scale DIC [18,19] has shown potential for analysis of small-scale damage such as fibre/matrix debonding in composites.

DIC detects the damage on the surface and reveals some data on the damage in the inner plies close to the surface ply [20–23], which is not sufficient in all cases. The detection of cracks in the inner plies is very difficult in CFRP composites, since they are not transparent. This is usually performed post-mortem, which allows crack closure due to stress relaxation as the test is interrupted and the specimen is removed for analysis. Thus, this should be performed *in-situ* to precisely track the progression of crack formation in the inner plies. Edge microscopy is a good supplementary technique for this purpose, as a complement for surface DIC. Previously, the authors applied a multi-instrument experimental approach to identify the damage modes and their progression in different QI CFRP specimens under plain tension

[22,23]. 2D DIC on the front surface was utilized simultaneously with *in-situ* edge microscopy and Acoustic Emission (AE) registration. It was possible to detect successfully different damage modes such as surface cracks, transverse cracks in inner plies and macro delaminations by 2D DIC at various scales. The application of *in-situ* edge microscopy provided data on matrix cracking and the consequent delaminations, showing reliable correlations with the registered AE events. Moreover, a multi-scale DIC analysis [24] could characterize the evolution of transverse cracks and its correlation with the presence of defects.

In this paper, the combination of 2D DIC on the surface and *in-situ* edge microscopy around the hole are applied for damage characterisation in four different QI CFRP laminates during OHT tests. The simultaneous utilization of *in-situ* edge microscopy and 2D DIC allows for detection of intra-laminar damage in the inner plies (matrix cracks in the 90° and ±45° plies), inter-laminar damage in the inner plies (delaminations at ±45°/90° interfaces) and damage on the surface plies. These observations provide reliable explanations for the features noted in the corresponding stress-strain curves. It is observed that the stacking sequence of the specimen influences the damage progression. Damage initiates as matrix cracks in the inner 90° plies or in the outer 90° or 45° plies, depending on the layup. It is found that DIC surface strain maps does not always show butterfly-shape concentrations around the hole, which is attributed to the anisotropic configuration of composites, as it is reported before in [16]. In some layups, strain concentration around the hole is not observed, but inter-laminar damage near the free edges causes excessive strain concentrations through the length. Sole DIC cannot detect this type of damage modes, but thanks to the *in-situ* edge microscopy, it can be identified and correlated with the stress-strain response of the laminates. The work adds to the existing data on damage progression during OHT test of QI laminates and reveals important features of the damage phenomena.

2. MATERIAL AND EXPERIMENTAL METHODOLOGY

2.1. Material and Test Specimens

Test specimens are made from *Hexcel's HexPly® UD AS4/8552 CFRP* prepregs. The fibre volume fraction and nominal thickness of the prepreg are 57.4 % and 0.184 mm, respectively. A 455 × 455 mm plate with a stacking sequence of $[+45_2/90_2/-45_2/0_2]_s$ is produced by curing in an autoclave using the manufacturer's recommended cure cycle [25]: 7 bar pressure throughout the whole cycle, 2 °C/min ramps and two holds at 120°C and 180°C for 1 and 2 hours, respectively. Then, smaller plates are cut from the manufactured plate with a water-cooled diamond saw to obtain 1) $[+45_2/90_2/-45_2/0_2]_s$, 2) $[90_2/-45_2/0_2/+45_2]_s$, 3) $[-45_2/0_2/+45_2/90_2]_s$, and 4) $[0_2/+45_2/90_2/-45_2]_s$ laminates, as shown in Figure 1.

Each small plate is cut to six tension specimens according to the dimensions provided in *ASTM D5766* [26] and *ASTM D3039* [27]. More specifically, dimensions of the specimens are 2.95 ± 0.09 mm thickness, 15.64 ± 0.25 mm width, 72.64 ± 1.54 mm gauge and 174.64 ± 2.54 mm total length. One edge of each specimen is grinded and polished for *in-situ* edge microscopy.

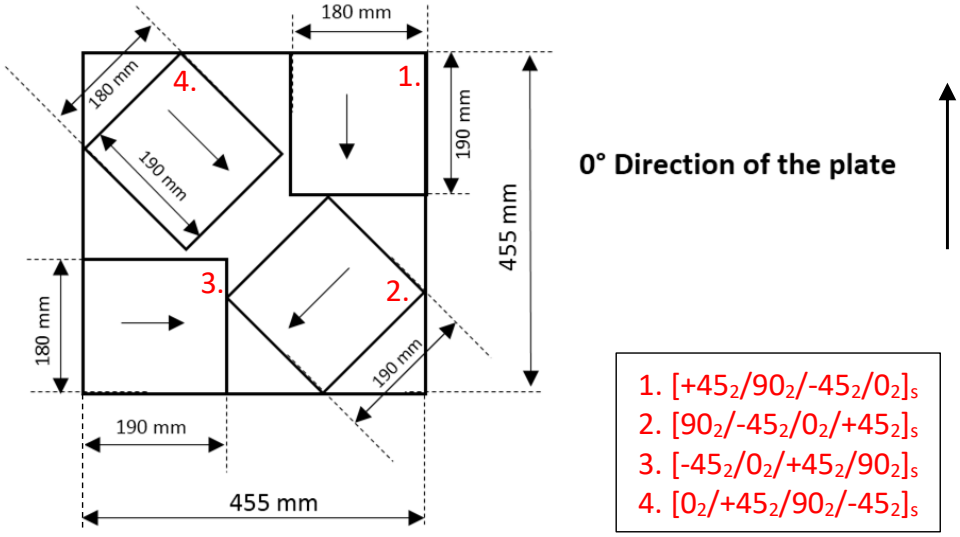

Figure 1. Manufactured $[+45_2/90_2/-45_2/0_2]_s$ plate with the cutting layout for obtaining specimens with different stacking sequences.

Test specimens can be considered as thick-ply laminates since the two adjacent plies with the same orientation form one single ply with a thickness of 0.368 mm. Thick-ply laminates are favourable for investigation of progressive failure, since they were found to experience multiple matrix and fibre damage modes with extensive delamination before failure [1–3,5,6].

A hole is made in the centre of each specimen. The hole has a diameter of 2.5 mm, satisfying the requirement of the width-to-diameter ratio of 6, prescribed in *ASTM D5766* [26]. The hole is drilled with a carbide drill bit. The specimen is placed on a wooden base to prevent damage when the drill bit leaves the specimen. A steel plate containing a hole of the same size as that of the specimen is placed on the specimen for determining the location of the hole. A calliper is used to align the hole of the steel exactly in the middle of the specimen. These three parts are fixed by the clamp table of the drilling machine along with a C-clamp to prevent vibration during drilling.

2.2. Open-Hole Tension Tests

OHT tests are performed with a deformation rate of 1 mm/min using an electro-mechanical *Instron 4505* universal test machine and according to the *ASTM D5766* standard [26]. Schematic view of the experimental arrangement is shown in Figure 2, and the details of the *in-situ* observation techniques are given in the further subsections.

Six OHT tests were carried out for each laminate type. One of them is performed until failure. This is labelled as “UTS test” (UTS = Ultimate Tensile Stress). The aim of UTS test is to determine the critical stress/strain level for each layup. The other five tests are stopped just after the critical stress level. For each laminate type, two out of the five tests are performed with both surface DIC and *in-situ* edge microscopy (full analysis tests), whereas for the remaining three tests only surface DIC is applied. The description of the tests and their damage detection methodology are summarized in Table 1. The full analysis tests for the [-

$45_2/0_2/+45_2/90_2]_s$, $[90_2/-45_2/0_2/+45_2]_s$ and $[0_2/+45_2/90_2/-45_2]_s$ laminates are with a final stress of 95%, 90% and 85% % of the UTS respectively and $[+45_2/90_2/-45_2/0_2]_s$ laminate is the test with the two load drops. The reason for not choosing the 95% of the UTS in each specimen type is because it is seen that the damage saturates after the aforementioned stress levels.

Table 1. Summary of the test description and the applied damage detection methodology for each laminate type.

Laminate Type	**Final stress level with respect to UTS***	**Applied methodology**
$[-45_2/0_2/+45_2/90_2]_s$	100 %	
	70%	DIC
	75%	DIC
	80%	DIC
	90%	DIC & Edge microscopy
	95%	DIC & Edge microscopy
$[90_2/-45_2/0_2/+45_2]_s$	100 %	
	70%	DIC
	75%	DIC
	80%	DIC
	90%	DIC & Edge microscopy
	95%	DIC & Edge microscopy
$[0_2/+45_2/90_2/-45_2]_s$	100 %	
	70%	DIC
	75%	DIC
	80%	DIC
	85%	DIC & Edge microscopy
	95%	DIC & Edge microscopy
$[+45_2/90_2/-45_2/0_2]_s$	100 %	
	70%	DIC
	75%	DIC
	80%	DIC
	1st Load Drop	DIC & Edge microscopy
	2nd Load Drop	DIC & Edge microscopy

2.3. Digital Image Correlation

DIC is used for measuring local strains and detecting cracks in the surface plies, intra-ply cracks in the adjacent plies and macro-delaminations between the interfaces of the inner plies, same as in the authors' previous study [22–24]. A random speckle pattern, required for DIC, is sprayed on one surface of the specimens. *In-situ* images are captured by a *LIMESS* high-speed Charge-Coupled Device (CCD) camera with the *VIC-Snap* software. The imaging rate is 2 s^{-1} and the resolution of the images is 1392 × 1040 pixels (55 x 41 mm^2). *VIC-2D* software is used for DIC calculations. A 30 × 14 mm^2 region on the specimen surface is selected in the software as the area of interest, with the hole subtracted from it. An schematic view of the area of interest on the speckled region is shown in Figure 2. DIC subset and step sizes are set to 21 and 4 pixels (0.835 x 0.159 mm^2), respectively. DIC is performed with *normalized square differences* criterion, *optimized 4-tap interpolation*, and *Gaussian subset weights*. Lagrangian strain maps are computed, which can be used to identify the surface cracks and delaminations.

2.4. *In-situ* Edge Microscopy

In-situ edge microscopy is applied as a second damage detection technique, allowing observation of the polished edge of the specimen during the test. A *LIMESS* CCD camera with extension tubes (for magnification) is used to acquire images, with the same rate as that of the surface camera (2 s^{-1}). This technique allows to focus on a 5 × 3 mm (1392 × 1040 pixels) study zone on the polished edge of the specimen. Through this analysis intra- and inter-laminar damage modes through the laminate thickness are detected.

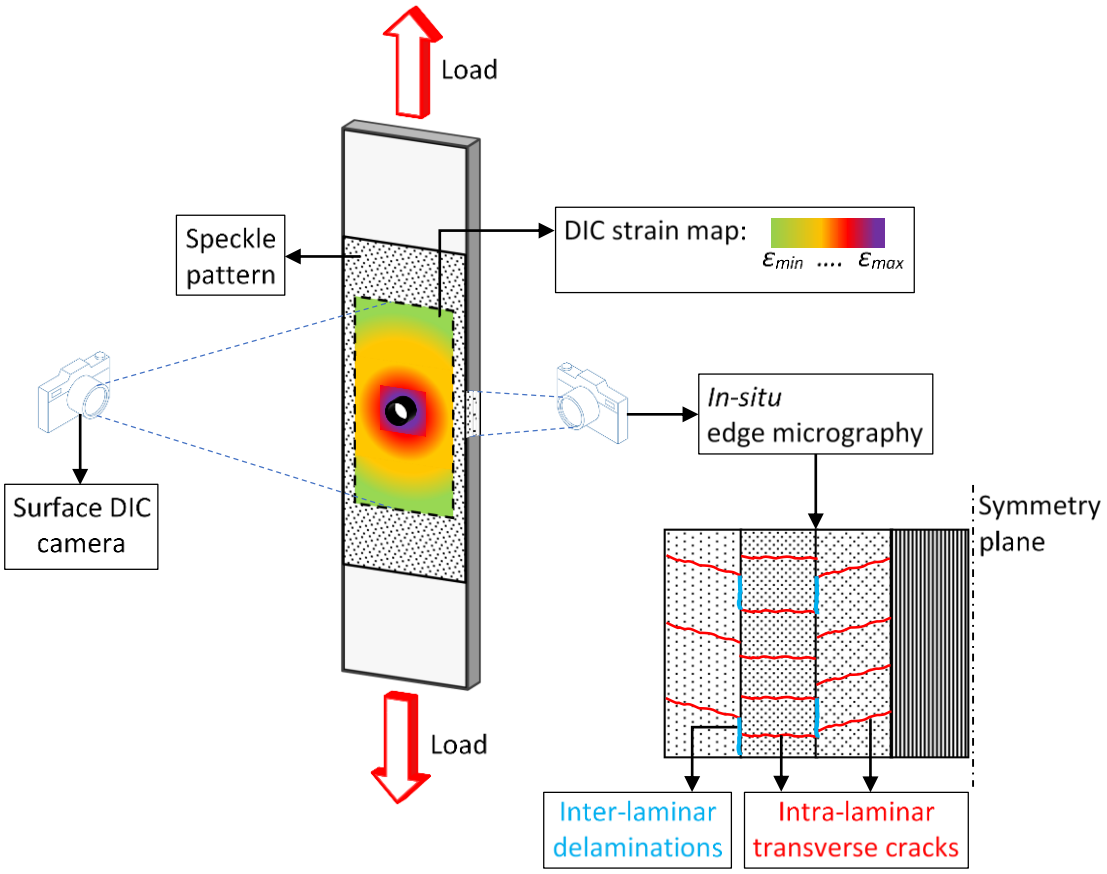

Figure 2. Schematic view of the experimental methodology.

3. RESULTS AND DISCUSSION

3.1. Final Failure Modes

Final failure modes of specimens at the end of UTS tests are shown in Figure 3. Large surface cracks around at the hole regions are seen in the $[+45_2/90_2/-45_2/0_2]_s$ and $[90/-45_2/0_2/+45_2]_s$ specimens. Large delaminations are present in the $[+45_2/90_2/-45_2/0_2]_s$ laminate too. Surface cracks in different regions of the surface of $[90/-45_2/0_2/+45_2]_s$ specimens are visible. Only a large surface crack is seen near the end tab in $[-45_2/0_2/+45_2/90_2]_s$ specimen. However, large free edge delaminations are present in this specimen type. Finally, ply splits and fibre breaks can be observed in $[0_2/+45_2/90_2/-45_2]_s$ specimen in Figure 3.

The distinguished final failure modes of each OH QI specimens suggest different initial damage modes and their progression throughout the tension tests. So, the damage progression in each specimen are presented in further sub-sections in details.

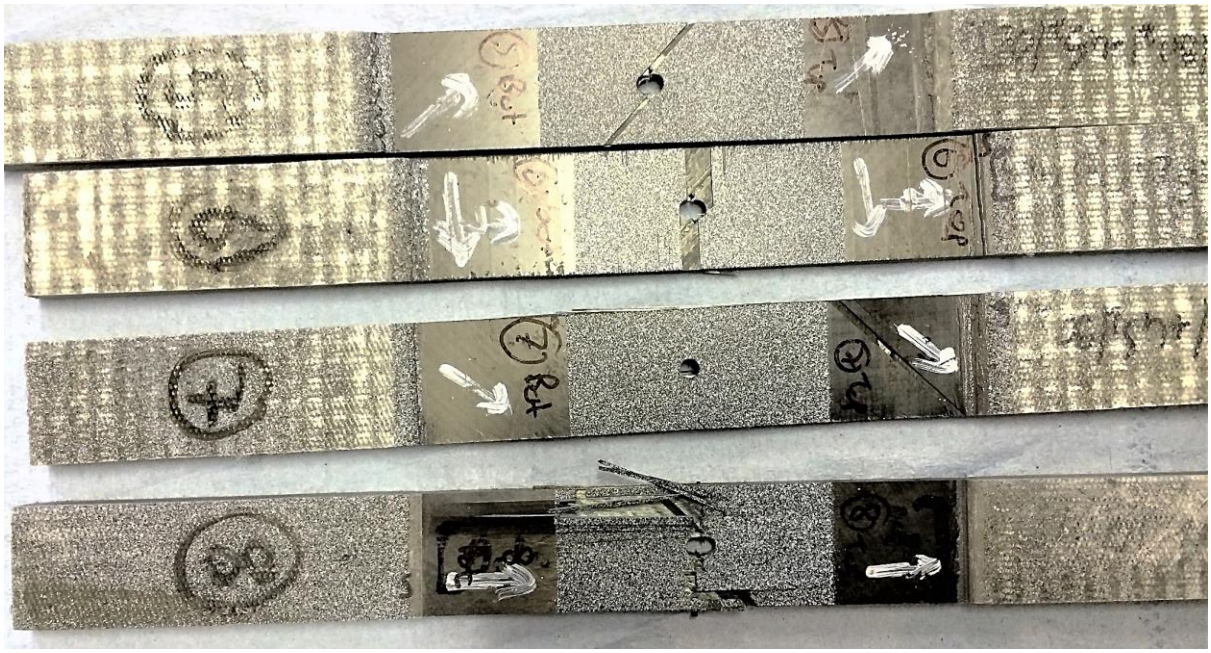

Figure 3. Final failure modes of specimens.

3.2. $[-45_2/0_2/+45_2/90_2]_s$ Laminate

The stress-strain curves corresponding to the six $[-45_2/0_2/+45_2/90_2]_s$ specimens are shown in Figure 4. The final stress levels and the damage observation tools in each test are given on the legend in Figure 4. The highlight in the legend of Figure 4 (TEST 5) represents the stress-strain curve corresponding to the damage progression shown in Figure 5. The aforementioned marking applies for the other laminate types in the next sections, as well.

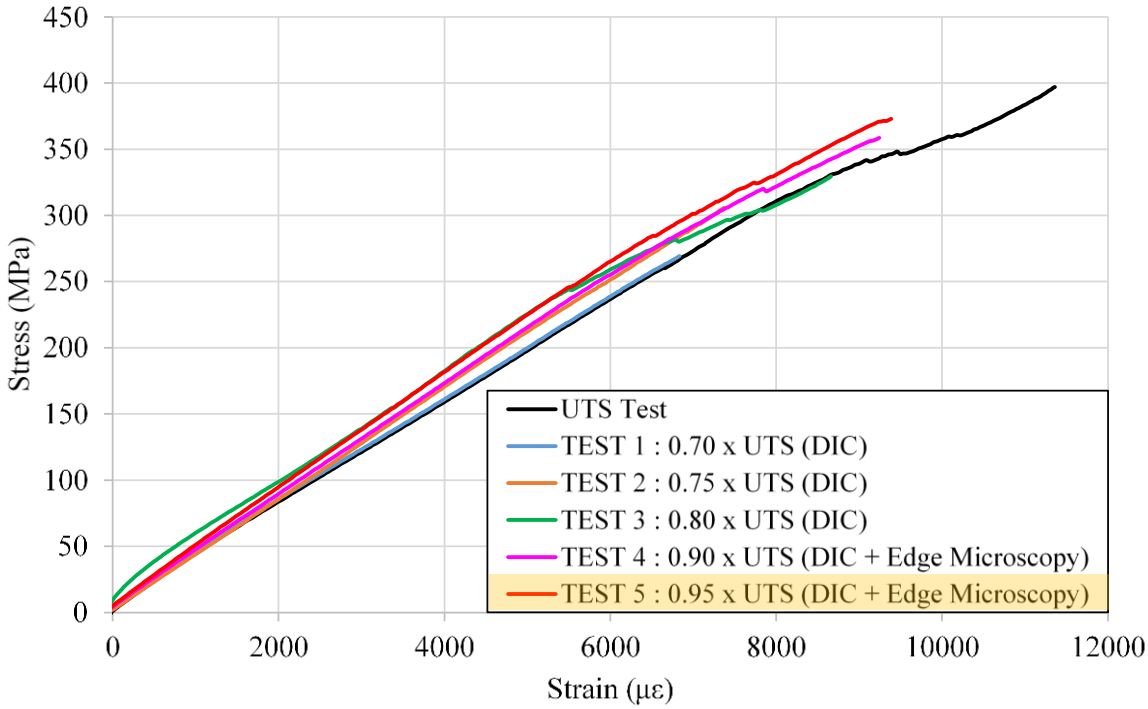

Figure 4. Stress-strain curves of the OHT test on the $[-45_2/0_2/+45_2/90_2]_s$ specimens – the highlight in the legend represents the stress-strain curve corresponding to the damage progression shown in Figure 5.

Figure 5 represents the damage detected via *in-situ* edge microscopy and surface DIC in a $[-45_2/0_2/+45_2/90_2]_s$ specimen. Different damage modes are indicated with different shapes, and the order of appearance of matrix cracks in 90° and +45° plies are shown with numbers. This marking is also used for the other laminate types in the next sections.

Damage progression in the $[-45_2/0_2/+45_2/90_2]_s$ specimen is detailed below.

1. Transverse matrix cracks in 90° plies. The first damage observed in the edge study zone is observed at 3500 με and it is a transverse crack in the 90° plies, shown with red rectangles in Figure 5. At this strain level, butterfly-shaped strain concentrations can be observed in the ε_1 DIC strain map around the hole, which might be due to a high deformation around the hole on the surface -45° plies.

2. Macro-delaminations at free edges. Butterfly-shape strain concentration around the hole becomes visible at 3500 με in the ε1 strain map. It expands through the edges until 6700 με as traced with the colour change from blue to green due to the increase in the strain gradient. There are blue regions remain at the tips of the hole, since the deformations at these regions are less, as expected. Meanwhile, the initiation of a macro-delamination at the top +45°/90° interface occurs from the free edge of the specimen (not the one being imaged). This is not observed in ε1 strain map but is detected in the ε2 strain map at 6700 με. This is the strain level, where a small load drop is observed in the stress-strain curve of the 5th test in Figure 4. The edge strain concentration in the transverse direction (ε2), highlighted with white rectangles in Fgure 5, is caused by higher Poisson's contraction due to the delamination at the +45°/90° interface. Sole DIC cannot identify the ply levels of delaminations but the use of edge microscopy and the reliable observations in authors' previous studies for plain tension tests [22,23] provides the evidence for determination of ply levels of macro-delaminations. It was seen that excessive deformation in ε2 strain maps corresponded to macro-delamination at the ±45°/90° interface of [-452/02/+452/902]s specimens [22,23].

3. Multiplication of matrix cracks; micro-delaminations. As observed in the edge study zone, the second transverse crack in the 90° plies occurs at 7600 με, together with two matrix cracks in the adjacent +45° plies (indicated in Figure 4 with yellow parallelograms) and micro-delaminations at the +45°/90° interface (shown with green rectangles).

4. Intensive macro-delamination; multiple matrix cracking. Two surface cracks are seen to occur around the hole, in the ε_1 strain map, at 6700 με and 7600 με. The red coloured strain concentrations correspond to the opening of the cracks in the surface -45° plies. Progression of the macro-delamination becomes intensive at 8200 με that is also the strain level at which another matrix crack in the +45° plies starts from the micro-delamination at the +45°/90° interface. The third transverse cracks in the 90° plies occurs at 9300 με along with another

matrix crack in the adjacent +45° plies. At this strain level, a macro-delamination near the observed free edge of the specimen becomes visible in the ε_2 strain map. This macro-delamination can correspond to those detected in the edge study zone (within white rectangles) at the end of the test (9400 με). It is worth noting that the cracks in the 90° plies have planes almost normal to the loading direction, while the cracks' planes in the 45° plies make an angle of ~45° with the loading direction.

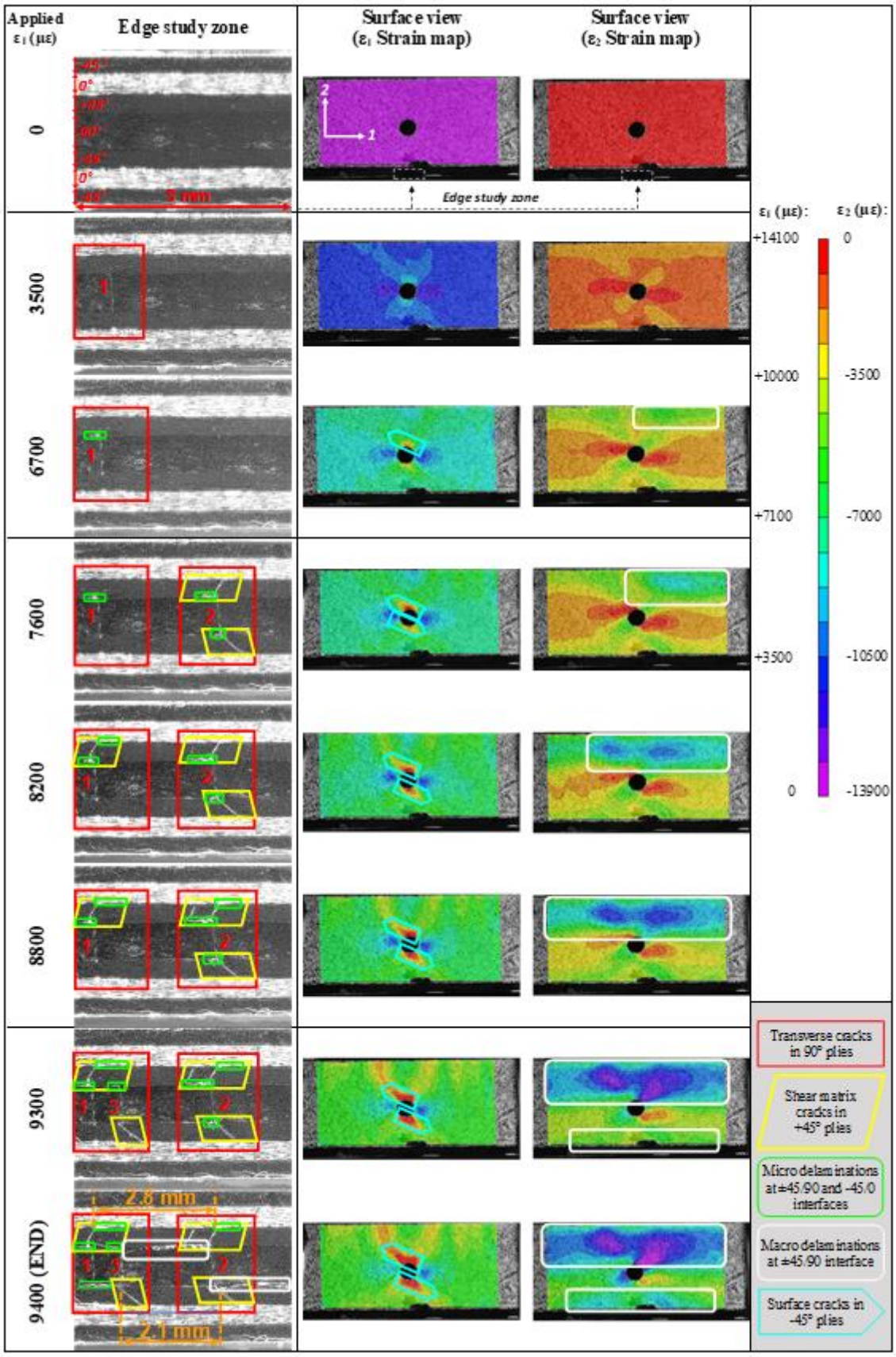

Figure 5. Damage detected via *in-situ* edge microscopy and surface DIC in the $[-45_2/0_2/+45_2/90_2]_s$ laminate – the numbers in the edge views show the order of the appearance of the damage mode in the study zone.

3.3. $[90_2/-45_2/0_2/+45_2]_s$ Laminate

Laminates consisting of 90° plies on the surface are favourable for DIC analysis of transverse cracks on the surface because numerous transverse cracks form in the surface 90° plies as the applied load increases [14,24]. The stress-strain curves corresponding to the six tension tests on the $[90_2/-45_2/0_2/+45_2]_s$ specimens are shown in Figure 6. 4th test is chosen for investigation of damage progression (presented in Figure 7).

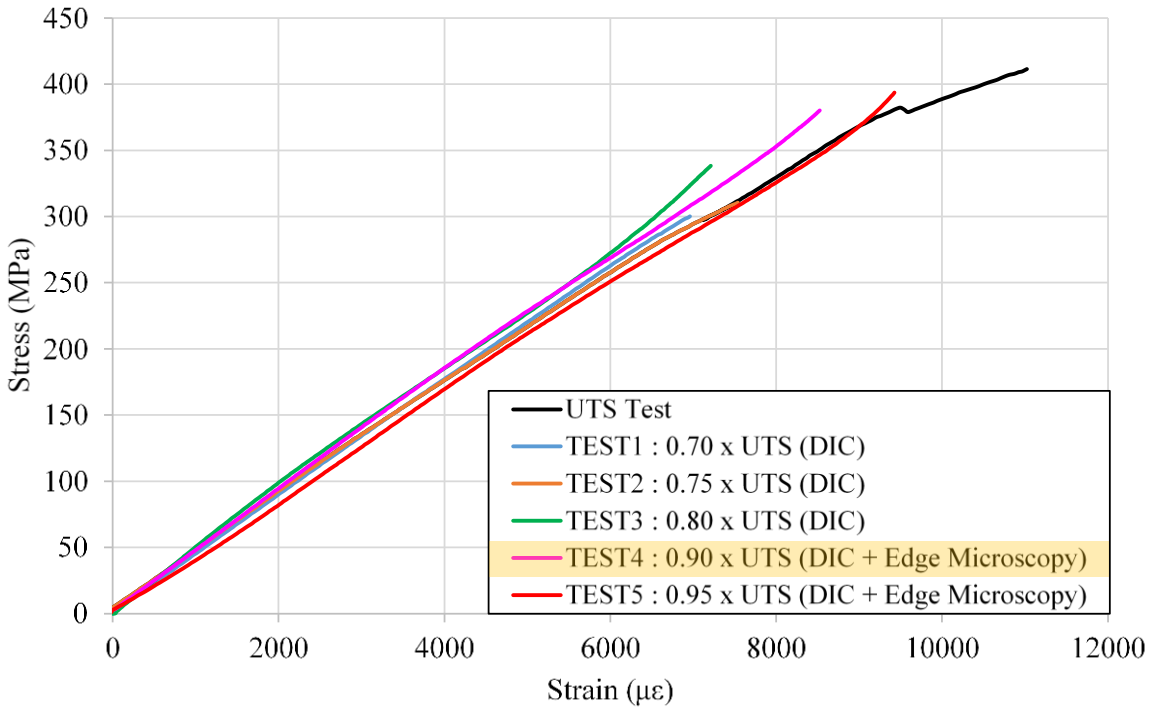

Figure 6. Stress-strain curves of the OHT test on the $[90_2/-45_2/0_2/+45_2]_s$ specimens – the highlight in the legend represents the stress-strain curve corresponding to the damage progression shown in Figure 7.

In this laminate type, the following damage modes are observed.

1. Transverse matrix cracks in 90° and shear-matrix cracks -45° plies. Even though it is not very clear, the first transverse crack at the edge study zone is detected in the bottom 90° plies at 3700 με, indicated with the red rectangle in Figure 7. The first detected transverse crack on the surface plies appear at the hole, at 4500 με, as detected in the ε_1 strain map. It propagates

and becomes visible in the edge study zone at 4700 με. This provides a correlation between the *in-situ* edge microscopy and DIC surface observation. Two matrix cracks are detected in the -45° plies in the edge observation zone. One initiates in the bottom -45° plies from the transverse crack in the adjacent ply at 6800 με, but does not propagate much before 8500 με. The other matrix crack appears in the top -45° plies, at 7800 με.

2. Delaminations. High deformations occur around the hole as expected and they are clearly detected in the ε_2 strain map in Figure 7 at 4700 με. It was found, for the $[-45_2/0_2/+45_2/90_2]_s$ laminate type, that larger Poisson's contraction caused by inter-laminar delaminations at +45°/90° interfaces near the free edge leads to excessive deformations in the ε_2 strain map (blue – purple colours). However, edge delaminations are not observed in $[90_2/-45_2/0_2/+45_2]_s$ specimens and the transverse deformations at the edges are zero in the ε_2 strain map as seen in Figure 7. In fact, large strain concentrations (purple zones) occur around the hole in $[90_2/-45_2/0_2/+45_2]_s$ specimens. The propagation of the surface transverse crack at 4700 με causes delamination from the adjacent -45° ply, initiating the macro-delamination at the 90°/-45° interface, as can be noticed in the ε_2 strain map (Figure 7). In the edge study zone only one micro-delamination at the top 90°/-45° interface is detected, at 6800 με but the macro-delaminations are not detected since they do not propagate to the edges and are only remained around the hole.

3. Multiple surface cracks. Multiplication of surface transverse cracks are observed in the ε_1 strain map after 6800 με. Only two surface cracks (one in each surface) are observed in the edge study zone. This is because the zone length (5 mm) is rather small compared to the crack spacing of ~ 3 crack/mm. DIC detects seven surface cracks until 90 % of the UTS, which gives a crack spacing of ~ 7 crack/mm.

It is important to note that the matrix cracks in the inner -45° plies initiate from the transverse cracks in the 90° plies. However, the 0° plies next to the -45° plies prevent the matrix cracks to propagate into the +45° plies. Unfortunately, large delaminations occur only around the hole but they are not observed in the edge study zone in this laminate type. It could be that large delaminations occur at strain levels beyond 8500 με, corresponding to the load drop in the “UTS test”, shown in Figure 6.

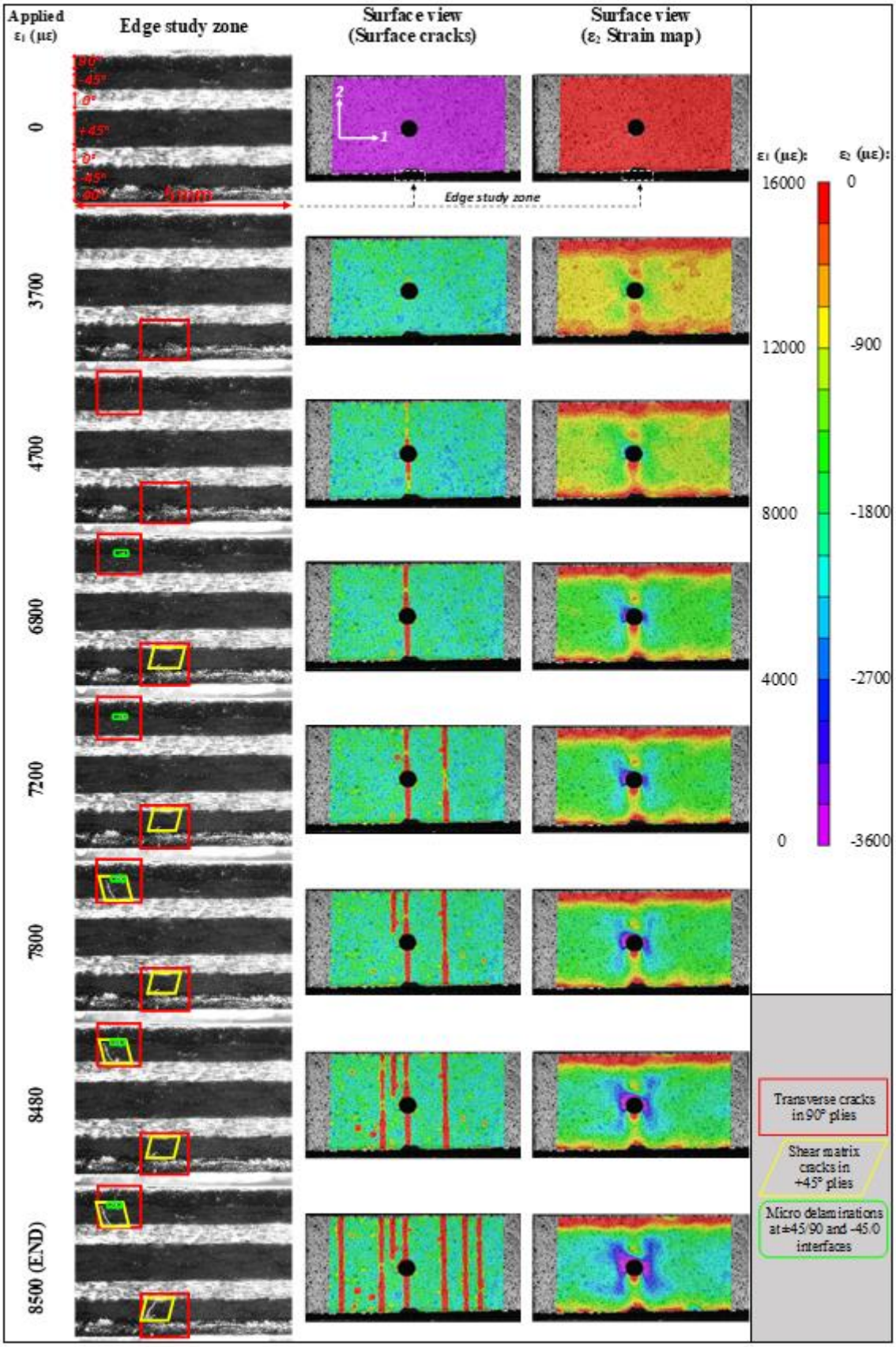

Figure 7. Damage detected via *in-situ* edge microscopy and surface DIC in the $[90_2/-45_2/0_2/+45_2]_s$ laminates – the numbers in the edge views show the order of the appearance of the damage mode in the study zone.

3.4. $[0_2/+45_2/90_2/-45_2]_s$ Laminate

Stress-strain responses of the six $[0_2/+45_2/90_2/-45_2]_s$ specimens are plotted in Figure 8. 4th test is chosen for the analysis of damage progression, which is presented in Figure 9, where the order of matrix cracks in the 90° and ±45° plies is labelled.

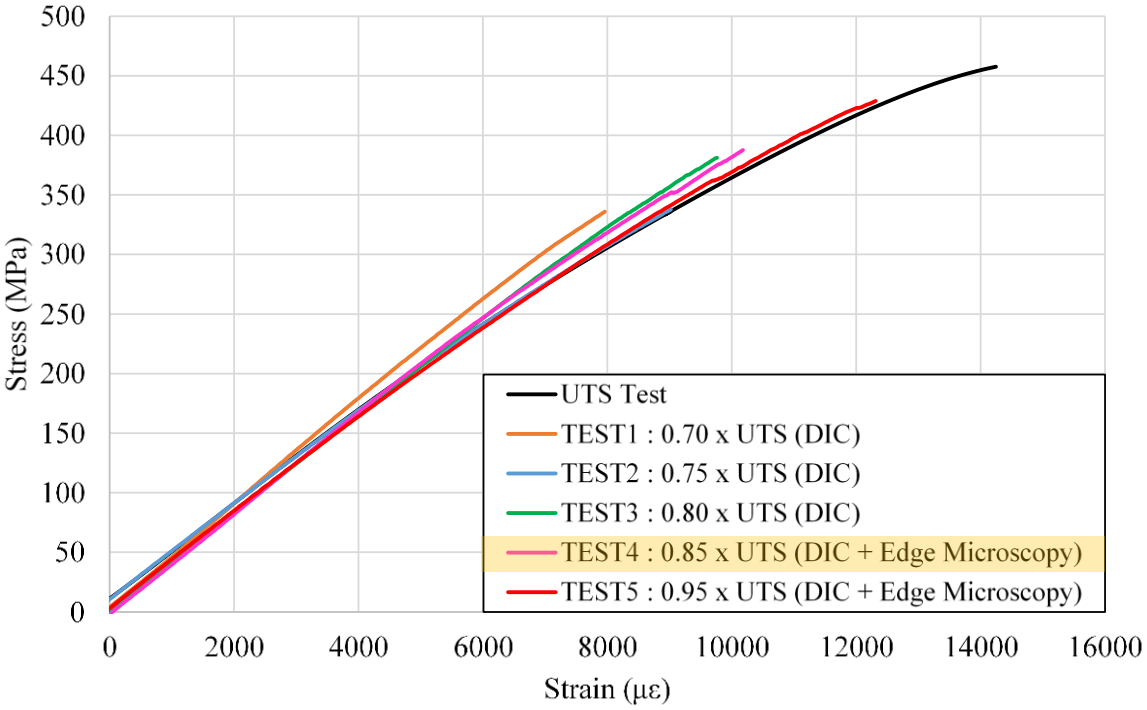

Figure 8. Stress-strain curves of the OHT test on the $[0_2/+45_2/90_2/-45_2]_s$ specimens – the highlight in the legend represents the stress-strain curve corresponding to the damage progression shown in Figure 9.

The characterized stages of damage progression are described, below.

1. Transverse cracks in 90° plies. The first transverse crack is observed at 5800 με in the edge study zone (Figure 9). Since it is away from the DIC surface, it does not cause any distortion in the strain map. The presence of the 0° plies on the surface causes different shape of concentrations around the hole in the ε_1 and ε_2 strain maps. The second transverse crack in the same 90° ply is observed at 6600 με.

2. Matrix cracks in +45° plies. Initiation of a matrix crack in the top +45° plies can be noted in correspondence with a micro-delamination in the top +45°/90° interface at 6600 με. It propagates through the ply thickness and becomes visible in the edge study zone at 7400 με, as shown in Figure 9. Two matrix cracks appear in the bottom +45° plies and in the middle -45° plies at 8800 με and 8900 με, respectively. Only the views at 8900 με are presented in Figure 9 for the sake of brevity. They both initiate from the micro-delamination corresponding to the transverse cracks in the adjacent 90° plies.

3. Splitting in surface 0° plies. Damage initiation next to hole can be observed in the ε_1 and ε_2 strain maps at 7400 με in Figure 9. The areas with very low values in the ε_2 strain map are considered to be splitting through the specimen's length, which are indicated with light-blue coloured pentagon shapes.

4. Multiplication of transverse cracks in 90° plies. 8900 με is the critical strain level for the $[0_2/+45_2/90_2/-45_2]_s$ laminates in terms of multiplication of transverse cracks. Because of the intensive transverse cracking, the test is stopped at 85 % of the UTS, corresponding to an applied strain of 10180 με. Formation of cracks in the ±45° and 90° plies bring about micro-delaminations at their interfaces, as indicated with small, green rectangles in Figure 9.

5. Macro-delaminations. The high deformation (blue-purple areas) detected around the hole in the ε_2 strain map (Figure 9) at 8900 με is assumed to be associated with macro-delaminations between the inner plies that propagate mainly along the 45° direction. The macro-delaminations do not appear in the edge study zone.

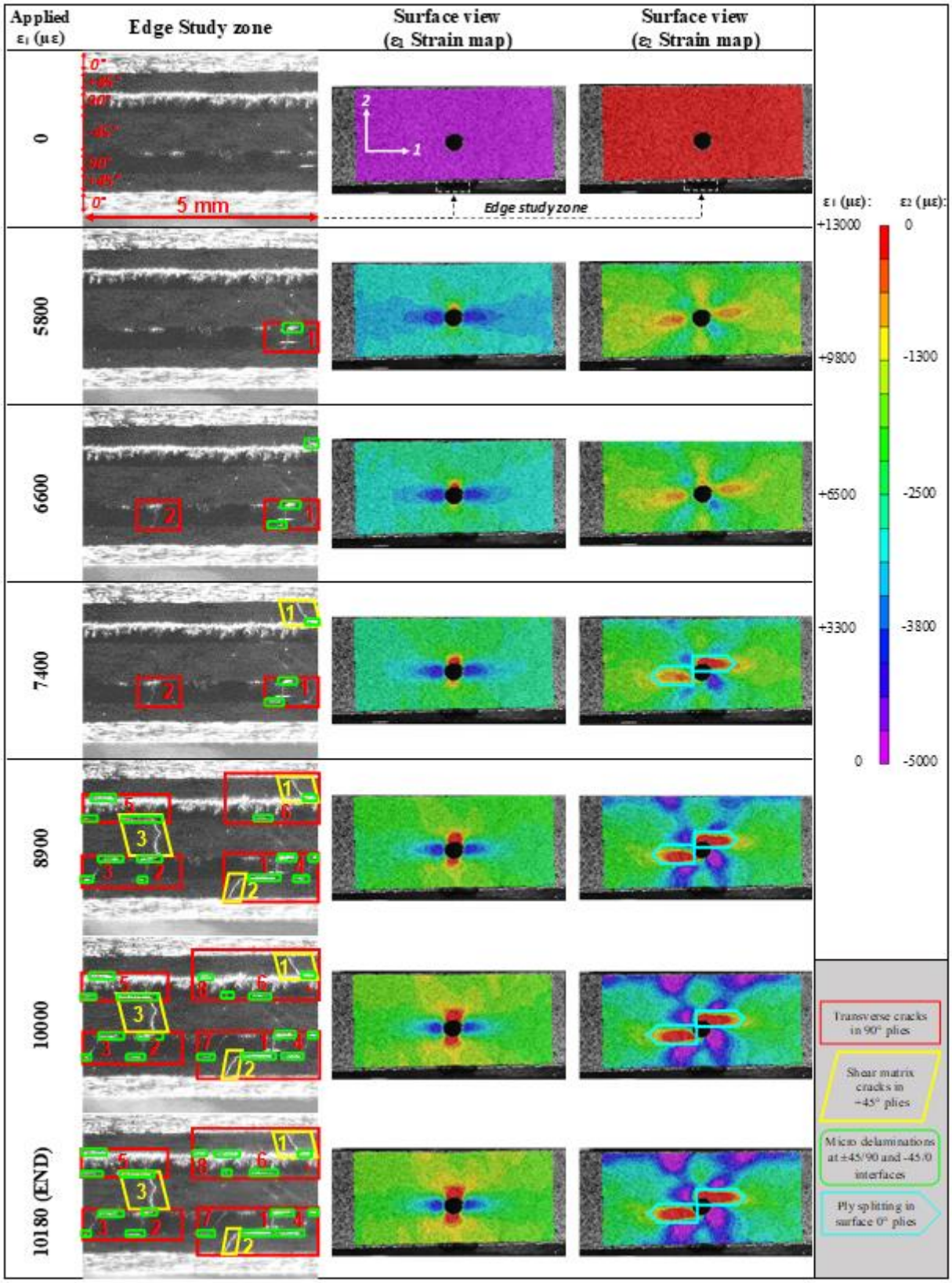

Figure 9. Damage detected via *in-situ* edge microscopy and surface DIC in the $[0_2/+45_2/90_2/-45_2]_s$ laminate – the numbers in the edge views show the order of the appearance of the damage mode in the study zone.

3.5. $[+45_2/90_2/-45_2/0_2]_s$ Laminate

The stress-strain curves corresponding to the six $[+45_2/90_2/-45_2/0_2]_s$ specimens are presented in Figure 10. The large load drops may be due to macro-delaminations. 5th test is chosen for exploration of damage progression, detailed in Figure 11.

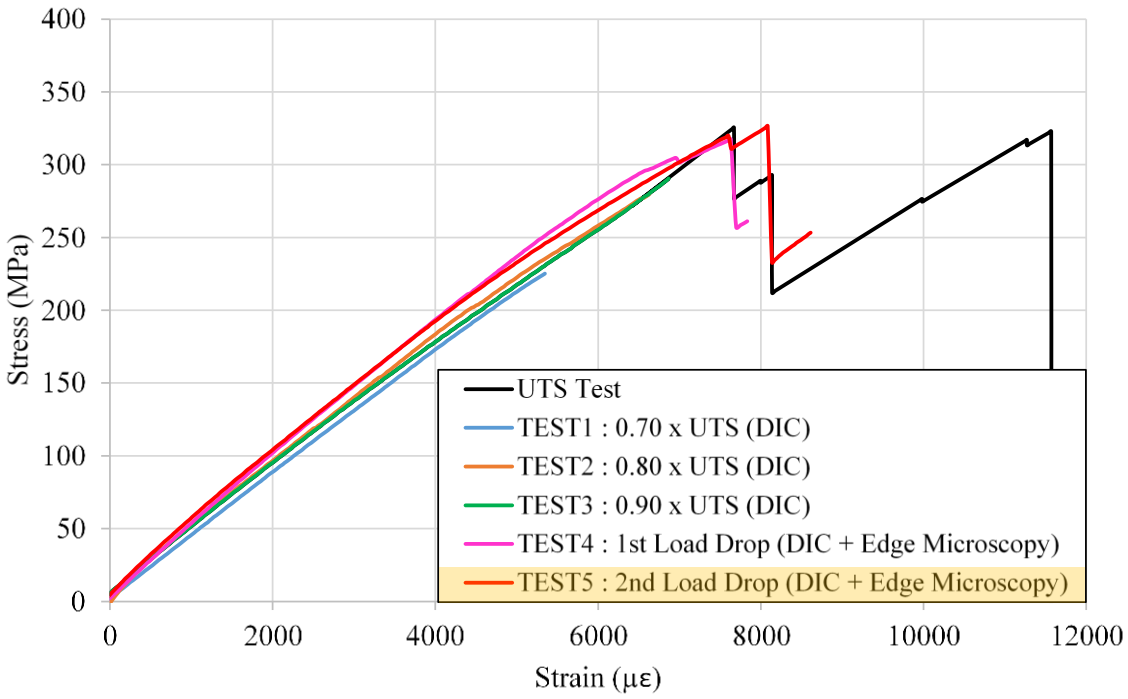

Figure 10. Stress-strain curves of the OHT test on the $[+45_2/90_2/-45_2/0_2]_s$ specimens – the highlight in the legend represents the stress-strain curve corresponding to the damage progression shown in Figure 11.

The damage progression scenario is explained below.

1. Matrix cracks in surface +45° plies. First damage is a surface crack in the top +45° plies, starting from the hole, as observed in the ε_1 strain map, at 4800 με (Figure 11). The surface crack propagates towards the free edge of the specimen at 5300 με, when another matrix crack is found to initiate from the hole, on the opposite side.

2. Macro-delaminations. A free edge delamination in an underlying interface is detected at 4800 με, which is indicated with a white rectangle in the ε_2 strain map in Figure 11. It is

highly possible that this free edge delamination occurs due to the transverse cracks at the inner 90° plies, but they are not observed in the edge study zone. The delamination starts propagation from 4800 με and approaches the hole. Meanwhile, similar strain concentrations in different directions appear around the hole and propagate until 7600 με, as shown with the white rectangle in Figure 11.

3. Transverse matrix cracks in 90° and shear-matrix cracks in the inner ±45° plies. The first transverse crack in the 90° plies is detected in the edge study zone, at 7000 με (Figure 11). Afterwards, the tip of a macro-delamination is observed at the bottom -45°/90° interface and propagates until 7600 με. Moreover, as noted in the ε_1 strain map, the surface crack propagates toward the monitored edge of the specimen between 7100 – 7600 με.

4. Multiplication of matrix cracks and macro-delaminations. Several matrix cracks are observed in the 90° and -45° plies within the edge study zone, at 7600 με (Figure 11). It is believed that multiplication of the cracks in the surface +45° or inner -45° plies causes macro-delaminations at ±45°/90° interfaces. Two macro-delaminations are observed at the top -45°/90° interface in the edge study zone, at 7700 με. These cause the first load drop in the stress-strain curve of 5th test, as noted in Figure 10. More macro-delaminations at the bottom ±45°/90° interfaces appear at 8100 με, which correspond to the second and the largest load drop in 5th test, as shown in Figure 10.

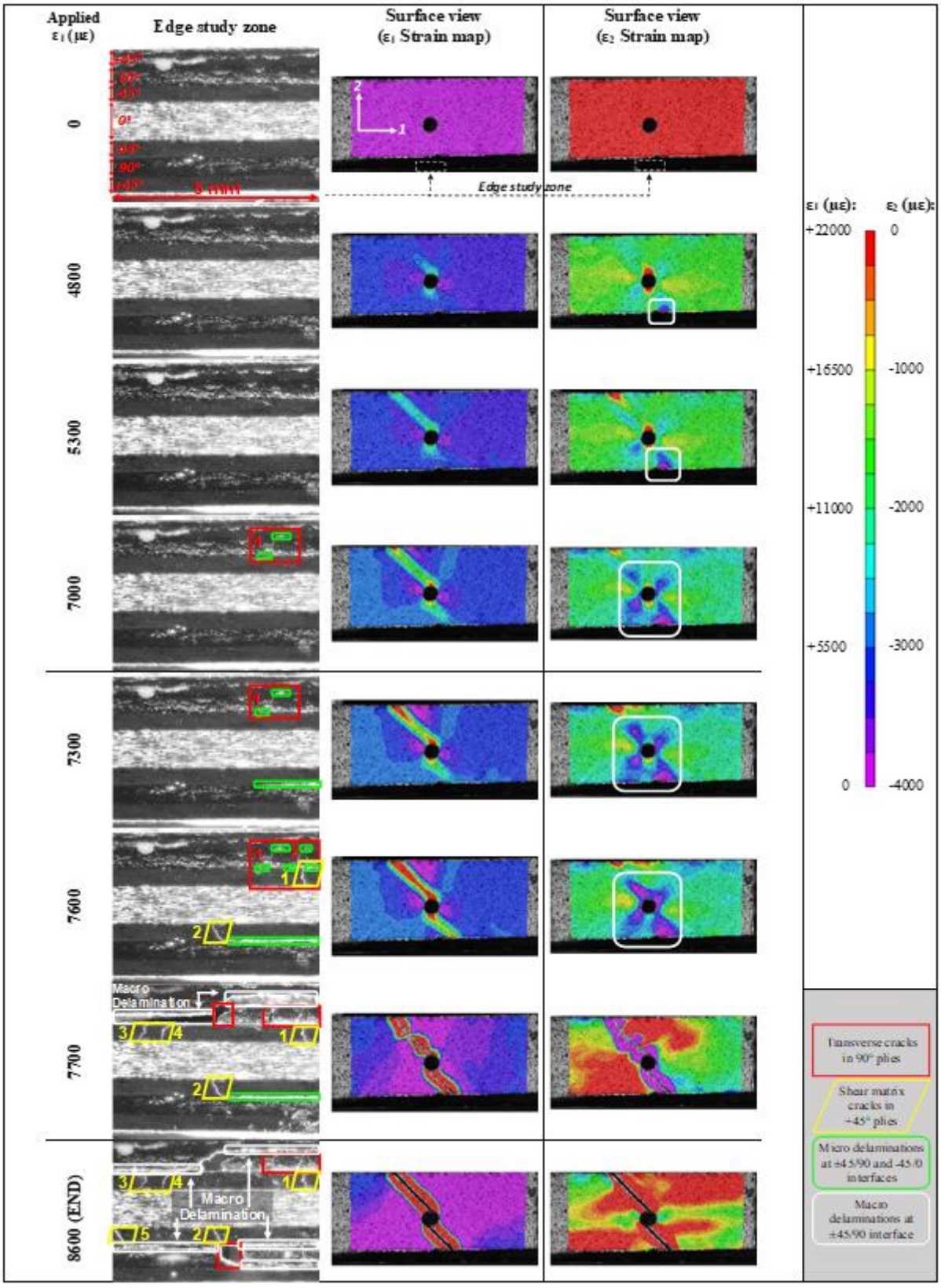

Figure 11. Damage detected via *in-situ* edge microscopy and surface DIC in the $[+45_2/90_2/-45_2/0_2]_s$ laminate – the numbers in the edge views show the order of the appearance of the damage mode in the study zone.

3.6. Summary of Damage Progression Scenarios

Details of damage progression in OHT tests of QI laminates with different layups are discussed in Sections 3.1 – 3.4. It is very possible that Classical Lamination Theory (CLT) or a simple numerical model would predict same failure levels through the loading for each laminate. However, the simultaneous application of DIC and *in-situ* edge microscopy proves that damage initiation and propagation depends considerably on the stacking sequence. Therefore, the study of the damage in OH QI laminates is complex and asks for use of different damage observation techniques to identify different damage modes. Strain threshold level corresponding to the first observation of each damage mode in each layup is presented in Figure 12. Such data on the damage mode threshold has not been reported in the previous studies of OHT of QI laminates. It is an important outcome that can serve for choosing the optimal layup in design of laminated structures with open-holes.

Figure 12 shows that transverse cracking in 90° plies is usually the first damage mode to be observed. They appear at the same time with micro-delaminations. This happens very early (at around 3500 με) when the 90° plies are the outer or middle plies, respectively due to the free surface effect and higher ply thickness. Large number of transverse and shear matrix cracks, in the inner 90° and +45° plies, and their quick propagation through the length of the specimen leads to large free edge macro-delaminations in the $[-45_2/0_2/+45_2/90_2]_s$ specimen. On the other hand, the transverse crack through the width of $[90_2/-45_2/0_2/+45_2]_s$ specimen and the possible localized shear-matrix cracks around the hole, leads to macro-delaminations at this region. The former laminate type may also have delaminations around the hole, but they cannot be visible in the strain maps in the presence of very large deformations near the free edges. In most cases, shear-matrix cracks in ±45° plies are detected, next.

The *in-situ* damage observation reveals that, in each laminate type, the propagation of different damage modes becomes intensive at certain strain levels, where the number of

observed damage mode increase rapidly. These strain levels are named “intensive damage threshold” in Figure 12. It is found that 7800 με is the intensive damage threshold level for the $[90_2/-45_2/0_2/+45_2]_s$ laminate and the only observed damage after this strain level is multiplication of surface cracks. On the other hand, propagation of matrix cracks and the progression of large delaminations are seen to continue in the $[-45_2/0_2/+45_2/90_2]_s$ laminate after the intensive damage level (8800 με).

Damage threshold level of the $[0_2/+45_2/90_2/-45_2]_s$ specimen is 5800 με. First observed damage in the $[0_2/+45_2/90_2/-45_2]_s$ specimen is a transverse cracks in the 90° plies and the second one shear-matrix cracks in the ±45° plies. The surface damage in the $[0_2/+45_2/90_2/-45_2]_s$ is observed at 7400 με due to splitting of the surface 0° plies. Intensive damage level is found to be 8800 με, due to large number of matrix cracks in the 90° and ±45° plies, and delaminations as found in the edge study zone at its intensive damage level (8900 με).

The first damage mode in the $[+45_2/90_2/-45_2/0_2]_s$ laminate is surface crack in the +45° plies at 4800 με. The initiation of surface cracks immediately leads to macro-delaminations at the +45°/90° interface. Multiple number of damage modes are observed at the intensive damage level in the $[+45_2/90_2/-45_2/0_2]_s$ laminate (7700 με). Large load drops are observed in the stress-strain curve of the $[+45_2/90_2/-45_2/0_2]_s$ laminate due to the macro-delaminations interfaces at 7700 με and 8100 με.

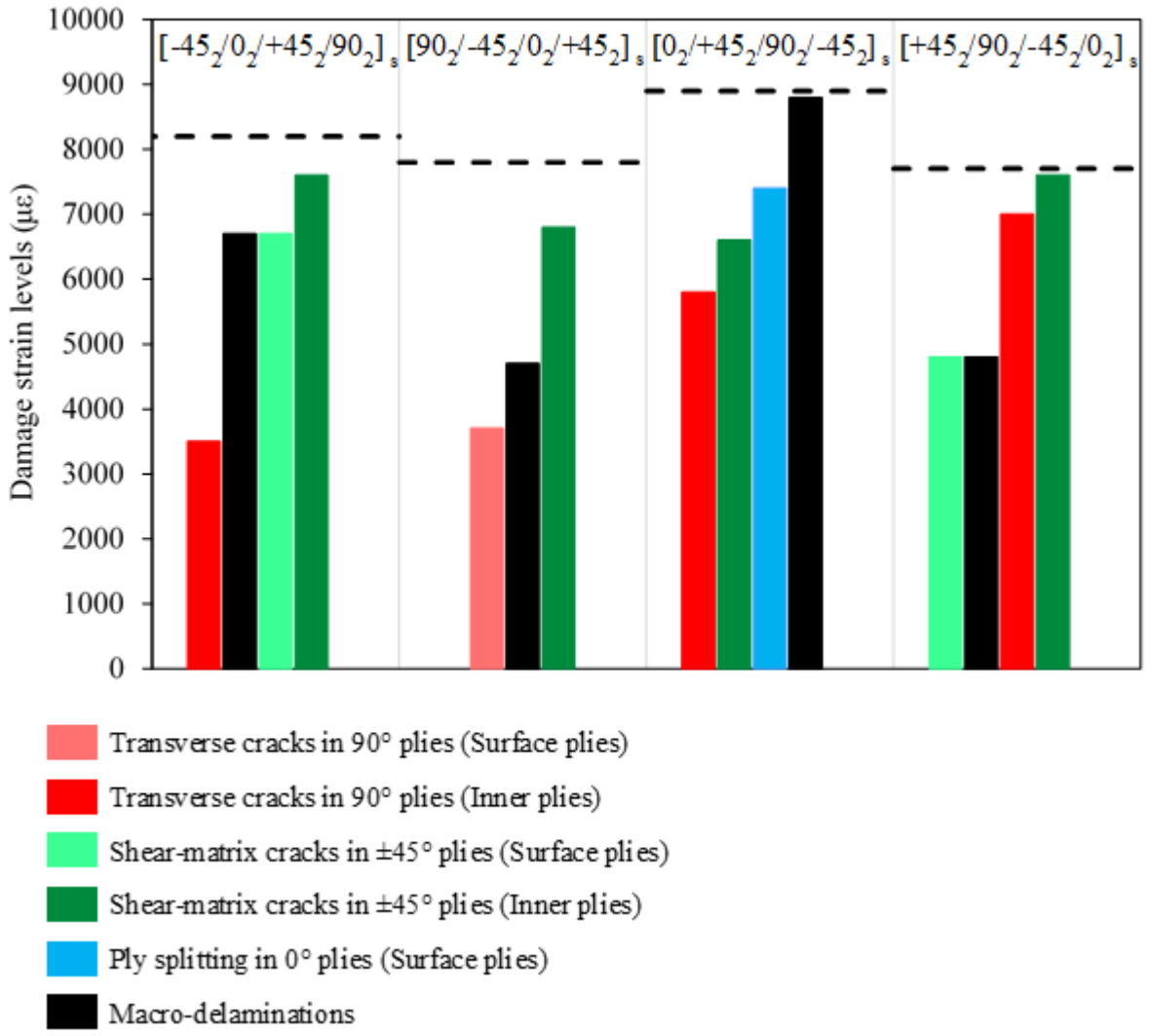

Figure 12. Strain thresholds of damage mode in different QI laminates.

4. CONCLUSION

This study proves the efficiency of simultaneous utilization of 2D DIC and *in-situ* edge microscopy techniques for identification of damage progression in OHT QI CFRP specimens. It adds *in-situ* evidence to the existing data on the damage progression in previously studied $[+45_2/90_2/-45_2/0_2]_s$ laminates [1–6], by providing quantitative and comparative information on the damage modes thresholds, and reveals new features of the damage phenomena in three more QI layups: $[-45_2/0_2/+45_2/90_2]_s$, $[90_2/-45_2/0_2/+45_2]_s$ and $[0_2/+45_2/90_2/-45_2]_s$. It is found that while damage initiates within the inner plies of the $[-45_2/0_2/+45_2/90_2]_s$ and $[0_2/+45_2/90_2/-45_2]_s$ specimens, surface cracks are the first to appear in $[90_2/-45_2/0_2/+45_2]_s$ and $[+45_2/90_2/-$

$45_2/0_2]_s$ laminates. Initiation and progression of different damage modes are explored in the edge study zones and DIC surface strain maps. The *in-situ* observations provide links between the damage modes and the changes in the stress-strain curves. It is found that large load drops in the stress-strain curve of the $[+45_2/90_2/-45_2/0_2]_s$ laminate do not necessarily happen due to inter-laminar delaminations of -45°/0° interfaces, but the ±45°/90° delaminations are the reason.

It is very possible that Classical Lamination Theory (CLT) or a simple numerical model would predict same failure levels through the end of loading. However, the simultaneous application of DIC and *in-situ* edge microscopy proves the difference in damage progression in each laminate, as shown in this study. It means that the outcomes of this study can serve for choosing the correct lamination for design purposes.

Even though the optical tools provide strong evidences for correlation of damage modes with stress-strain curves, the initiation of damage modes may happen earlier than they are observed. In order to accurately determine their initiation and increase the robustness of the damage mode identification, more real-time analysis tools, such as, acoustic emission technique can be used for the same loading condition. Thus, the next study will include the application of AE technique with optical tools. Then, the applied combined methodology can be extended for different loading conditions to detect damage modes.

5. ACKNOWLEDGEMENT

Authors acknowledge the support of the Boğaziçi University Research Fund, Istanbul Development Agency (ISTKA), and TUBITAK BIDEB 2214-A under project codes 10020/15A06D3, ISTKA/BIL/2012/58 and 1059B141600673 respectively. S.V. Lomov holds the Toray Chair on Composites at KU Leuven, the support of which is gratefully

acknowledged. Participation of M. Mehdikhani was supported by the KU Leuven Research Council, project C24/17/052.

6. REFERENCES

[1] Green BG, Wisnom MR, Hallett SR. An experimental investigation into the tensile strength scaling of notched composites. Compos Part A Appl Sci Manuf 2007;38:867–78. doi:10.1016/j.compositesa.2006.07.008.

[2] Wisnom MR, Hallett SR. The role of delamination in strength, failure mechanism and hole size effect in open hole tensile tests on quasi-isotropic laminates. Compos Part A Appl Sci Manuf 2009;40:335–42. doi:10.1016/j.compositesa.2008.12.013.

[3] Hallett SR, Green BG, Jiang WG, Wisnom MR. An experimental and numerical investigation into the damage mechanisms in notched composites. Compos Part A Appl Sci Manuf 2009;40:613–24. doi:10.1016/j.compositesa.2009.02.021.

[4] Wisnom MR, Hallett SR, Soutis C. Scaling Effects in Notched Composites. J Compos Mater 2010;44:195–210. doi:10.1177/0021998309339865.

[5] Nixon-pearson OJ, Hallett SR, Withers PJ, Rouse J, Harper PW, Kawashita LF. Damage development in open-hole composite specimens in fatigue . Part 1 : Experimental investigation. Compos Struct 2013;106:882–9. doi:10.1016/j.compstruct.2013.05.033.

[6] Nixon-Pearson OJ, Hallett SR. An investigation into the damage development and residual strengths of open-hole specimens in fatigue. Compos Part A Appl Sci Manuf 2015;69:266–78. doi:10.1016/j.compositesa.2014.11.013.

[7] Mollenhauer D, Iarve E V., Kim R, Langley B. Examination of ply cracking in composite laminates with open holes: A moiré interferometric and numerical study. Compos Part A Appl Sci Manuf 2006;37:282–94. doi:10.1016/j.compositesa.2005.06.004.

[8] Ifju PG, Han B. Recent Applications of Moiré Interferometry. Exp Mech 2010;50:1129–47. doi:10.1007/s11340-010-9404-9.

[9] Caminero MA, Lopez-Pedrosa M, Pinna C, Soutis C. Damage monitoring and analysis of composite laminates with an open hole and adhesively bonded repairs using digital image correlation. Compos Part B Eng 2013;53:76–91. doi:10.1016/j.compositesb.2013.04.050.

[10] Caminero MA, Lopez-Pedrosa M, Pinna C, Soutis C. Damage assessment of composite structures using digital image correlation. Appl Compos Mater 2014;21:91–106. doi:10.1007/s10443-013-9352-5.

[11] Sawan HA, Walter ME, Marquette B. Unsupervised learning for classification of acoustic emission events from tensile and bending experiments with open-hole carbon fiber composite samples. Compos Sci Technol 2015;107:89–97. doi:10.1016/j.compscitech.2014.12.003.

[12] Pierron F, Green B, Wisnom MR, Hallett SR. Full-field assessment of the damage process of laminated composite open-hole tensile specimens. Part II: Experimental

results. Compos Part A Appl Sci Manuf 2007;38:2321–32. doi:http://dx.doi.org/10.1016/j.compositesa.2007.01.019.

[13] Pierron F, Green B, Wisnom MR. Full-field assessment of the damage process of laminated composite open-hole tensile specimens. Part I: Methodology. Compos Part A Appl Sci Manuf 2007;38:2307–20. doi:http://dx.doi.org/10.1016/j.compositesa.2007.01.010.

[14] Erçin GH, Camanho PP, Xavier J, Catalanotti G, Mahdi S, Linde P. Size effects on the tensile and compressive failure of notched composite laminates. Compos Struct 2013;96:736–44. doi:https://doi.org/10.1016/j.compstruct.2012.10.004.

[15] Aidi B, Case SW. Experimental and Numerical Analysis of Notched Composites Under Tension Loading. Appl Compos Mater 2015;22:837–55. doi:10.1007/s10443-015-9439-2.

[16] Dai S, Cunningham PR, Marshall S, Silva C. Open hole quasi-static and fatigue characterisation of 3D woven composites. Compos Struct 2015;131:765–74. doi:10.1016/j.compstruct.2015.06.032.

[17] Furtado C, Arteiro A, Catalanotti G, Xavier J, Camanho PP. Selective ply-level hybridisation for improved notched response of composite laminates. Compos Struct 2016;145:1–14. doi:https://doi.org/10.1016/j.compstruct.2016.02.050.

[18] Mehdikhani M, Aravand M, Sabuncuoglu B, Callens MG, Lomov S V., Gorbatikh L. Full-field strain measurements at the micro-scale in fiber-reinforced composites using digital image correlation. Compos Struct 2016;140:192–201. doi:10.1016/J.COMPSTRUCT.2015.12.020.

[19] Mehdikhani M, Matveeva A, Aravand MA, Wardle BL, Lomov S V., Gorbatikh L. Strain mapping at the micro-scale in hierarchical polymer composites with aligned carbon nanotube grafted fibers. Compos Sci Technol 2016;137:24–34. doi:10.1016/J.COMPSCITECH.2016.10.021.

[20] Schorer N, Sause MGR. Identification of Failure Mechanisms in Cfrp Laminates Using 3D Digital Image Correlation. Proc 20th Int Conf Compos Mater ICCM-20, Copenhagen, Denmark 2015:19–24.

[21] Sause MGR. In Situ Monitoring of Fiber-Reinforced Composites Theory, Basic Concepts, Methods, and Applications. 2016.

[22] Oz FE, Ersoy N, Lomov S V. Do high frequency Acoustic emission events always represent fibre failure in CFRP laminates? Compos Part A Appl Sci Manuf 2017;103:230–5. doi:10.1016/j.compositesa.2017.10.013.

[23] Oz FE, Ersoy N, Mehdikhani M, Lomov S V. Multi-Instrument In-Situ Damage Monitoring in Quasi-isotropic CFRP Laminates Under Tension. Compos Struct 2018;196:163–80. doi:10.1016/j.compstruct.2018.05.006.

[24] Mehdikhani M, Steensels E, Standaert A, Vallons KAM, Gorbatikh L, Lomov S V. Multi-scale digital image correlation for detection and quantification of matrix cracks in carbon fiber composite laminates in the absence and presence of voids controlled by the cure cycle. Compos Part B Eng 2018;154:138–47. doi:10.1016/j.compositesb.2018.07.006.

[25] Hexcel. HexPly ® 8552 - Product Data Sheet - EU Version 2016:1–6.

[26] ASTM. D5766/5766M: Standard Test Method for Open-Hole Tensile Strength of Polymer Matrix Composite. Annu B ASTM Stand 2013;13:1–7. doi:10.1520/D5766.

[27] ASTM. D3039/D3039M: Standard Test Method for Tensile Properties of Polymer Matrix Composite Materials. Annu B ASTM Stand 2014;14:1–13. doi:10.1520/D3039.